Magnetic structure and hysteresis in hard magnetic nanocrystalline film: Computer simulation

Yongmei M. Jin and Yu U. Wang
Department of Ceramic and Materials Engineering, Rutgers University, 607 Taylor Road, Piscataway, New Jersey 08854

Andrei Kazaryan and Yunzhi Wang
Department of Materials Science and Engineering, The Ohio State University, 2041 College Road, Columbus, Ohio 43210

David E. Laughlin
Department of Materials Science and Engineering, Carnegie Mellon University, Pittsburgh, Pennsylvania 15213

Armen G. Khachaturyan[a)]
Department of Ceramic and Materials Engineering, Rutgers University, 607 Taylor Road, Piscataway, New Jersey 08854

(Received 17 May 2002; accepted 5 August 2002)

Three-dimensional micromagnetic simulations are used to study the effect of crystallographic textures on the magnetic properties of uniaxial nanocrystalline films of hard magnetic materials with arbitrary grain shapes and size distributions. The correlation lengths (effective ferromagnetic exchange interaction radius and domain wall width) are assumed to be smaller than the typical grain size. The Landau–Lifshitz equations of magnetization dynamics are employed to describe the distribution of magnetization in ferromagnetic domains, domain evolution during magnetization switching, and the hysteresis curve. The equations are solved numerically in reciprocal space using the fast Fourier transform technique. Simulations are performed for films of different grain textures. The results show that magnetic coupling between grains in thin films significantly affects the morphology of the magnetic domains and their response to the magnetic field applied. The greater the deviation of the uniaxial directions of the grains from the film normal, the smaller the coercivity and the remanence magnetization. It is also shown that the remanence magnetization and coercivity respond differently to the variations in film texture and that the magnetic reversal process is a collective process involving groups of grains. In particular, it is found that the crystallographic texture of the grains has a more complicated effect on the coercivity than on the remanence magnetization and on the character of topological changes during the magnetization reversal process. [DOI: 10.1063/1.1510955]

I. INTRODUCTION

In recent years the demand for high density recording media has led to intensive research in the area of hard magnetic materials whose properties can be controlled at smaller size scales. Typically, the materials used in media applications are polycrystalline thin films. Storing information on smaller and smaller length scales requires a significant reduction of the characteristic grain size, which makes the effect of grain microstructure an important issue for designing magnetic recording media. There are many factors that influence the magnetic properties of a nanocrystalline film, e.g., the grain size and grain orientation distributions, the grain shapes, the thickness of the film and the grain boundary properties. Due to the complexity of the relationship between these parameters and the magnetic properties, experimental studies have serious difficulty in providing a complete understanding of the principles that control the magnetic properties of nanocrystalline thin films. In such a situation a theoretical prediction of the outcomes of material processing becomes crucial. However, the potential of the analytical approach is limited to only a few cases with a good deal of simplification. For complicated cases such as the magnetic switching in polycrystalline films, the effects of both long-range magnetostatic interaction and short-range exchange interaction on the assemblies of anisotropic grains lead to complex collective behavior. It is clear that the only way to obtain a realistic theoretical description of magnetic systems of this complexity is by computational modeling based on micromagnetic dynamics.

Micromagnetic modeling has been extensively used to study the magnetization process in soft and hard magnetic materials. There are two common approaches—to solve the governing differential equations using finite element methods with adaptive meshing,[1,2] or to solve the Landau–Lifshitz equations where fast Fourier transform (FFT) is commonly employed over regular grids.[3–5] In this work we adopt the latter approach. We solve the Landau–Lifshitz equations in

[a)]Author to whom correspondence should be addressed; electronic mail: khach@jove.rutgers.edu

reciprocal space. The reason for this choice is twofold: (i) the reciprocal space formulation of the problem allows us to utilize the FFT algorithm, which is computationally efficient and ideal for parallel processing and, thus, allows us to simulate a large model size within a reasonable time frame; and (ii) this approach can be readily extended to take into account magnetostriction by incorporating the well-developed phase field microelasticity (PFM) theory and models, which solve the exact elastic interaction in solid state phenomena that involve elasticity.[6] Because of difficulties in solving elasticity equations that describe the elastic strain generated by arbitrary configuration of magnetic domains, there have not been any realistic simulations where the magnetostriction has been taken into account.

It should be noted that the reciprocal space representation of the Landau–Lifshitz equation, which includes the magnetostatic energy contribution, is conceptually and mathematically similar to the reciprocal space representation of the PFM equations, which include the strain energy contribution—the latter is based on the time-dependent Ginzburg–Landau equations. The PFM approach, which has been successfully employed for realistic simulations of diffusional and martensitic phase transformations, dislocation plasticity and crack evolutions,[7] can be easily integrated into the micromagnetic dynamics, thereby extending the range of problems that can be theoretically addressed. In particular, it opens the way to simulate more realistic ferromagnetic phenomena where magnetostriction is taken into account. In addition, various defects—magnetic defects such as imperfect grain boundaries and impurities as well as elastic defects such as misfitting precipitates and dislocations—can be easily integrated into this formalism. Extension of the theory is underway.

Ferromagnetic thin films for magnetic storage have been studied intensively using micromagnetic modeling (see Refs. 3–5 for recent reviews). So far these studies have been performed for magnetic materials with single domain grains or for two-dimensional problems where the magnetization variation along the film thickness is neglected. These assumptions are applicable for commonly used thin film media: currently most thin film media are of longitudinal type made of Co-based alloys, where the correlation length (effective ferromagnetic exchange interaction radius L_{ex} and domain wall width δ_W) are greater than the grain size or the film thickness. However these assumptions are not accurate enough to study the materials that could be candidates for a new generation of ferromagnetic media where the correlation lengths are comparable with the grain sizes or film thickness. Recently nanocrystalline perpendicular films with easy magnetization directions of grains close to the normal of the film and with high magnetocrystalline anisotropy are attracting the increased interest of researchers.[8–10] This is because the small grain size and perpendicular arrangement of the easy magnetization axis allow one to obtain greater recording densities, whereas the higher magnetocrystalline anisotropy increases the ferromagnetic thermal stability of the small grains. High anisotropy media like CoSm, CoPt and FePt whose anisotropy constants are an order of magnitude greater than those of the commonly used hexagonal-close-packed Co-based alloys are candidates for such films. Perpendicular films made of nanocrystalline hard ferromagnetic materials are still in the development stage, and existing experimental work is still limited. Thus, micromagnetic modeling by computer simulation would shed light on the basic principles controlling the structure–property relations, provide a better understanding of magnetic processes, and give insight into directions for future experimental research. This type of study is presented in this work. We have chosen a FePt polycrystalline thin film as an example of a very promising hard ferromagnetic material for perpendicular recording.

For hard magnetic materials the characteristic material length parameters, δ_W and L_{ex}, are of the order of several nanometers. These lengths are comparable with or even smaller than the grain sizes of nanocrystalline films. Under these circumstances, the assumption of single-domain grains is not always valid. Usually the thickness of a perpendicular film is greater than that of the longitudinal thin films—the film thickness of hard magnetic materials is usually of the order of several nanometers. Thus the variation of the magnetization vector along the film thickness cannot be neglected. In this article, the vector field of magnetization directions is described by an arbitrary three-dimensional (3D) distribution with no *a priori* constraints on this distribution or its evolution being imposed. The realistic 3D grain structure of the polycrystalline film is assumed to be a conglomerate of irregularly shaped grains. The shapes and sizes of grains affect the domain structure and magnetization within the domains because grain boundaries usually are sources of ''magnetic charges'' that generate the demagnetization field. This field can be especially strong near sharp edges and corners.

The effect of deviation of the easy axis of a grain from the applied field direction on the magnetic properties is comparatively easily characterized theoretically for a single grain situation. However, it is a much more complicated task for a polycrystal consisting of misaligned magnetically coupled grains. The magnetic coupling of the neighboring grains in the polycrystal occurs through exchange and magnetostatic interactions across the grain boundaries and thus it is affected by boundary imperfection. The higher the degree of perfection of the grain boundary structure, the higher the exchange interaction across the boundaries and thus the stronger the coupling between neighboring grains. Therefore, processing polycrystalline films with grain boundaries of different degrees of perfection is one of the ways to investigate how to achieve superior magnetic properties. Computer simulation is well suited to studying the effect of texture on the domain structure of polycrystalline film and its response to the magnetic field applied.

The purpose of this study is to investigate the effect of grain structure and its texture on the magnetic response of polycrystalline film to an applied magnetic field. In particular, we study the effects of texture on remanence magnetization, coercivity, and the hysteresis loop. All simulations are performed under the assumption that the grain boundaries are ideal in a sense that the exchange interaction across the grain boundaries is the same as in bulk and that the magnetic field is applied perpendicular to the film. In fact, lifting the

assumption of ideal boundaries would not considerably complicate the theory or affect the computational time.

II. MODEL

It is assumed that the evolution of the magnetization is described by the damping term of the Landau–Lifshitz dynamic equation[11]

$$\frac{d\mathbf{M}(\mathbf{r})}{dt} = -\alpha \frac{|\gamma|}{M(\mathbf{r})} \mathbf{M}(\mathbf{r}) \times [\mathbf{M}(\mathbf{r}) \times \mathbf{H}_{\text{eff}}(\mathbf{r})], \tag{1}$$

where $\mathbf{M}(\mathbf{r})$ is the magnetization density at point $\mathbf{r}$, $M(\mathbf{r})$ is its modulus, γ is the magnetomechanical ratio, α is the dimensionless damping parameter, and $\mathbf{H}_{\text{eff}}(\mathbf{r})$ is the effective vector magnetic field, which is a variational derivative of the system energy with respect to the magnetization,

$$\mathbf{H}_{\text{eff}}(\mathbf{r}) = -\frac{\delta E}{\delta \mathbf{M}(\mathbf{r})}. \tag{2}$$

The energy of the system is a sum of the exchange energy E_{exch}, the anisotropy energy E_{ani}, the magnetostatic energy E_{mag}, and the external field (Zeeman) energy E_{ext},

$$E = E_{\text{exch}} + E_{\text{ani}} + E_{\text{mag}} + E_{\text{ext}}. \tag{3}$$

A. Exchange energy

In this article we assume that the ferromagnetic material is far below the Curie point and that grain boundaries do not affect exchange interaction across the boundaries. Under these assumptions, the modulus of magnetization $M(\mathbf{r})$ is constant throughout the polycrystalline material and equal to the saturation magnetization, M_s, i.e., $M(\mathbf{r}) = M_s$. Then the exchange energy functional for a continuous distribution of the magnetization is

$$E_{\text{exch}} = A \int [\text{grad}\mathbf{m}(\mathbf{r})]^2 d^3r, \tag{4}$$

where A is the exchange stiffness constant, and $\mathbf{m}(\mathbf{r})$ is the vector field of magnetization directions,

$$\mathbf{m}(\mathbf{r}) = \frac{\mathbf{M}(\mathbf{r})}{M_s}. \tag{5}$$

In the case of imperfect grain boundaries, the exchange energy constant A is reduced near the boundaries and thus becomes coordinate dependent.

B. Anisotropy energy

In this article, we consider a uniaxial ferromagnetic material. The anisotropy energy of a grain with uniaxial magnetic symmetry is

$$E_{\text{ani}}(\mathbf{r}) = \int \{K_1 \sin^2[\theta(\mathbf{r})] + K_2 \sin^4[\theta(\mathbf{r})]\} d^3r, \tag{6}$$

where $\theta(\mathbf{r})$ is the angle between the anisotropy axis and magnetization direction, and K_1 and K_2 are energy density constants.

The equation for the anisotropy energy functional, Eq. (6), in a single crystal can be extended to a polycrystal comprised of grains having uniaxial magnetic symmetry. To do this, we have to introduce two vector fields that are presented in the same global coordinate system for all grains. One of them is the field of the direction, $\mathbf{p}(\mathbf{r})$, where $\mathbf{p}(\mathbf{r})$ is a unit vector that describes the distribution of the easy magnetization axes in all grains. By definition, $\mathbf{p}(\mathbf{r})$ is a constant in each grain and is different in different grains in accordance with the grain orientations. In fact, the field $\mathbf{p}(\mathbf{r})$ fully describes the grain geometry. The other field is the magnetization direction distribution function, $\mathbf{m}(\mathbf{r})$.

With these definitions, the anisotropy energy of a polycrystal can be presented in an invariant form as a functional of the magnetization direction, $\mathbf{m}(\mathbf{r})$, and the film texture characterized by the vector field $\mathbf{p}(\mathbf{r})$:

$$E_{\text{ani}} = \int (K_1\{1 - [\mathbf{p}(\mathbf{r}) \cdot \mathbf{m}(\mathbf{r})]^2\} + K_2\{1 - [\mathbf{p}(\mathbf{r}) \cdot \mathbf{m}(\mathbf{r})]^2\}^2) d^3r. \tag{7}$$

Equation (7) is valid under the assumption of a single-phase polycrystal with ''perfect'' grain boundaries. For the case of imperfect grain boundaries the energy density constants K_1 and K_2 at the boundaries are different from those inside grains, and thus coordinate dependent.

C. Magnetostatic energy

As is known, the magnetostatic energy can be presented as a sum of energies of interacting magnetic dipoles:

$$E_{\text{mag}} = \frac{1}{2} \int\int_{\mathbf{r} \neq \mathbf{r}'} \left[M_i(\mathbf{r}) \left(\frac{\delta_{ij}}{|\mathbf{r} - \mathbf{r}'|^3} - \frac{3(r_i - r_i')(r_j - r_j')}{|\mathbf{r} - \mathbf{r}'|^5} \right) M_j(\mathbf{r}) \right] d^3r d^3r', \tag{8}$$

where the integration is taken over the whole crystal body. Making use of the Fourier representations,

$$\mathbf{M}(\mathbf{r}) = \int \frac{d^3k}{(2\pi)^3} \mathbf{M}(\mathbf{k}) e^{i\mathbf{k}\cdot\mathbf{r}}, \tag{9a}$$

$$\frac{\delta_{ij}}{r^3} - 3\frac{r_i r_j}{r^5} = 4\pi \int \frac{d^3k}{(2\pi)^3} \frac{k_i k_j}{k^2} e^{i\mathbf{k}\cdot\mathbf{r}}, \tag{9b}$$

in Eq. (8), we have

$$E_{\text{mag}} = \tfrac{1}{2} \int \frac{d^3k}{(2\pi)^3} 4\pi \frac{|\mathbf{k}\cdot\mathbf{M}(\mathbf{k})|^2}{k^2} - \frac{1}{2} \int \frac{4\pi}{3} M^2(\mathbf{r}) d^3r. \tag{10}$$

The second term in Eq. (10) appears due to the constraint of excluding the terms $\mathbf{r} = \mathbf{r}'$ from the integration in Eq. (8). If we assume a constant magnetization modulus and use Eq. (5), the magnetostatic energy, Eq. (10), can be rewritten as

$$E_{\text{mag}} = \frac{1}{2} M_s^2 \int \frac{d^3k}{(2\pi)^3} 4\pi \frac{|\mathbf{k}\cdot\mathbf{m}(\mathbf{k})|^2}{k^2} - \frac{2\pi}{3} V M_s^2, \tag{11}$$

where the second term is a constant.

D. External field energy

The interaction energy of the magnetization with an external field $\mathbf{H}_{\text{ext}}$ is

$$E_{\text{ext}} = -\int \mathbf{H}_{\text{ext}} \cdot \mathbf{M}(\mathbf{r}) d^3 r. \tag{12}$$

By normalizing the vector $\mathbf{H}_{\text{ext}}$ with respect to M_s, $\mathbf{h}_{\text{ext}} = \mathbf{H}_{\text{ext}}/M_s$, and using Eq. (5), Eq. (12) can be rewritten as

$$E_{\text{ext}} = -M_s^2 \int \mathbf{h}_{\text{ext}} \cdot \mathbf{m}(\mathbf{r}) d^3 r. \tag{13}$$

E. Landau–Lifshitz equation

The total energy functional of an arbitrarily distributed magnetization in a uniaxial ferromagnetic polycrystal is a sum of the energies, Eqs. (4), (7), (11) and (13):

$$\begin{aligned} E = \int & \left(A[\text{grad}\mathbf{m}(\mathbf{r})]^2 + K_1\{1-[\mathbf{p}(\mathbf{r})\cdot\mathbf{m}(\mathbf{r})]^2\}\right. \\ & \left. + K_2\{1-[\mathbf{p}(\mathbf{r})\cdot\mathbf{m}(\mathbf{r})]^2\}^2\right) d^3 r \\ & + \frac{1}{2} M_s^2 \int \frac{d^3 k}{(2\pi)^3} 4\pi \frac{|\mathbf{k}\cdot\mathbf{m}(\mathbf{k})|^2}{k^2} - \frac{2\pi}{3} V M_s^2 \\ & - M_s^2 \int \mathbf{h}_{\text{ext}} \cdot \mathbf{m}(\mathbf{r}) d^3 r. \end{aligned} \tag{14}$$

It follows from Eqs. (2) and (14) that the normalized effective magnetic field, $\mathbf{h}_{\text{eff}} = \mathbf{H}_{\text{eff}}/M_s$, is

$$\begin{aligned} \mathbf{h}_{\text{eff}}(\mathbf{r}) = & 2\mathbf{p}(\mathbf{r})[\mathbf{m}(\mathbf{r})\cdot\mathbf{p}(\mathbf{r})] \\ & \times \left(\frac{K_1}{M_s^2} + 2\frac{K_2}{M_s^2}\{1-[\mathbf{m}(\mathbf{r})\cdot\mathbf{p}(\mathbf{r})]^2\}\right) + \mathbf{h}_{\text{ext}} \\ & - 2\frac{A}{M_s^2} \int \frac{d^3 k}{(2\pi)^3} k^2 \mathbf{m}(\mathbf{k}) e^{i\mathbf{k}\cdot\mathbf{r}} \\ & - \int \frac{d^3 k}{(2\pi)^3} 4\pi \frac{\mathbf{k}\cdot\mathbf{m}(\mathbf{k})}{k^2} \mathbf{k} e^{i\mathbf{k}\cdot\mathbf{r}}. \end{aligned} \tag{15}$$

Substituting Eq. (15) into Eq. (1) and using the normalized variables and $\mathbf{m}(\mathbf{r}) = \mathbf{M}(\mathbf{r})/M_s$ gives a reduced form of Eq. (1):

$$\frac{d\mathbf{m}(\mathbf{r})}{dt} = -\alpha|\gamma| M_s \mathbf{m}(\mathbf{r}) \times [\mathbf{m}(\mathbf{r}) \times \mathbf{h}_{\text{eff}}(\mathbf{r})]. \tag{16}$$

A solution of the nonlinear Eq. (16) with respect to $\mathbf{m}(\mathbf{r})$, in which $\mathbf{h}_{\text{eff}}$ is given by Eq. (15), fully describes the evolution of the domain structure.

III. RESULTS

In this simulation we assume that the magnetic field applied, $\mathbf{H}_{\text{ext}}$, is perpendicular to the film. It is convenient to present the coordinates and time in the kinetic equation in reduced form. To do so, we introduce the length unit l and time unit $\tau = (\alpha|\gamma|M_s)^{-1}$. Then the reduced spatial coordinates and reduced time are defined as

$$r_i^* = \frac{r_i}{l}, \quad t^* = \alpha|\gamma| M_s t. \tag{17a}$$

Equation (15) and thus the kinetic equation, Eq. (16), are governed by the following dimensionless parameters:

$$K_1^* = \frac{K_1}{M_s^2}, \quad K_2^* = \frac{K_2}{M_s^2}, \quad A^* = \frac{A}{M_s^2 l^2}. \tag{17b}$$

The material constants for FePt are given as $K_1 = 8 \times 10^7$ erg/cm^3, $M_s = 1140$ emu/cm^3, and $A = 1 \times 10^{-6}$ erg/cm. These material parameters yield the domain wall width $\delta_W = \pi\sqrt{A/K_1} = 3.5$ nm, the ferromagnetic exchange length $L_{\text{ex}} = \sqrt{A/4\pi M_s^2} = 2.5$ nm, the ratio of typical anisotropic energy to magnetostatic energy, $Q = 9.8$ ($Q = K_1/2\pi M_s^2$), and the ideal nucleation field $H_N^0 = 2K_1/M_s = 1.4 \times 10^5$ Oe. The ideal nucleation field H_N^0 is the external field required for homogeneous switching with no demagnetization factors, which also coincides with the coercivity since the hysteresis loop is square under such conditions. Its normalized value is $h_N^0 = H_N^0/M_s = 123$.

To reliably resolve the magnetic structure, the computational grid size l must be smaller than the characteristic lengths δ_W and L_{ex}. In the simulation we choose $l = 1.24$ nm. Substituting these parameters in Eq. (17b) and setting $K_2 = 0$ gives the dimensionless parameters as

$$K_1^* = 61.56, \quad K_2^* = 0, \quad A^* = 50. \tag{18}$$

The reduced time increment Δt^* is taken to be 0.001.

The geometry of the sample is assumed to be a laterally infinite film of finite thickness composed of a periodically repeated motif of 150 columnar grains with different orientations in the lateral X and Y directions. Therefore, the film consists of a periodically repeated configuration of 150 grains. This motif is our computational cell. Its structure is illustrated in Fig. 1(a). The size of the motif is about 159 nm$\times$159 nm, the thickness of the film is almost 10 nm, and the average grain size in the film plane is 10 nm.

This multigrain structure of the motif is generated by the so-called Voronoi tessellations[12] slightly modified to provide continuity of the grains at the periodic translation of the motif in the film plane. The procedure that generates the grains in the motif is briefly described as follows: (i) 150 seeds are randomly positioned on the film plane of the computational cell, and it is assumed that the plane is filled with periodic square cells; (ii) each point on the plane belongs to the grain whose seed is nearest to this point; (iii) the plane along the Z direction is stacked to make columnar grains with the thickness of films.

In the simulation, the kinetic equation, Eq. (16), is solved numerically in reciprocal space under periodic boundary conditions in three dimensions. The size of the computational cell is $128\times128\times128$, in other words, the computational region is discretized into 2 097 152 grid cells, where only 6.25% ($128\times128\times8$) of the cells is located inside the sample, and the rest are used as empty space to achieve accurate stray field effects. Simulations were performed with a parallel code running on NPACI supercomputers. The computational task in our code is highly parallel, where the key algorithm is the parallel 3D FFT. For the $128\times128\times128$ computational cell, we ran the parallel code with 2^n, say, 8, processors. We allocate 16 horizontal planes to each processor, first performing in-plane two-dimensional (2D) FFT followed by one-dimensional (1D) FFT along the vertical direction using NPACI FFT subroutines. In the latter step, we use

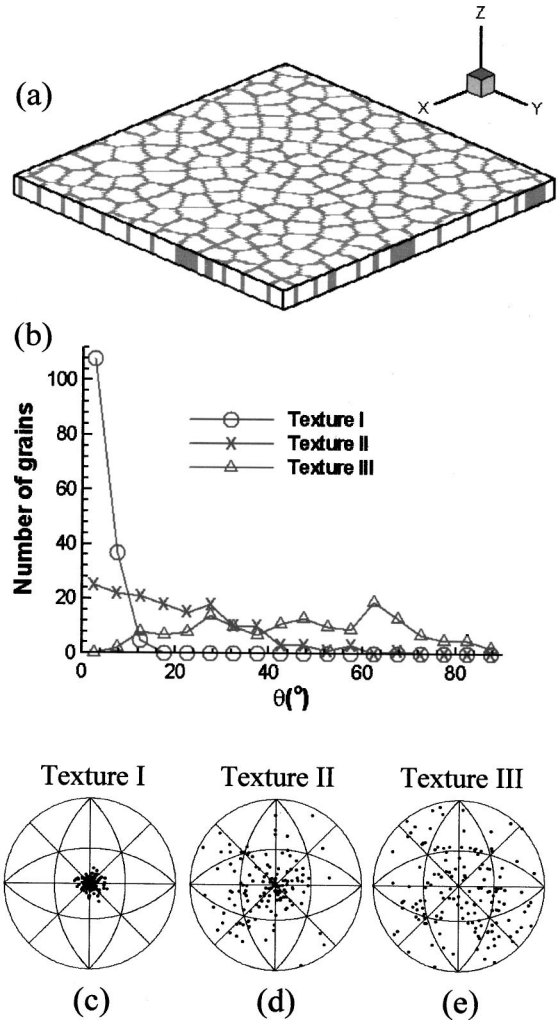

FIG. 1. (a) Polycrystalline structure of a film composed of 150 grains in the computational volume. (b) Distributions of uniaxial orientations of grains with respect to the *Z* direction for three grain textures. (c)–(e) Stereographic projections of grain uniaxial directions corresponding to the three grain textures, respectively.

message passing interface (MPI) to communicate among 8 processors and each processor takes care of 16 vertical planes. The efficiency of this process is very high. As a typical example, 2000 time steps with 8 processors takes 15 787 s according to a wall clock. This time is reduced to 8004 s with 16 processors, and further reduced to 4095 s with 32 processors. The other important advantage of this parallel structure is that the total simulation 3D array is distributed into 2^n processors, which allows us to simulate with a bigger system size under the limited memory of each single processor. This is important for a realistic simulation that requires a big simulation cell.

The simulations are performed for three examples of different crystallographic textures. The distribution angles between the uniaxial direction of the grains and the *Z* direction (film plane normal) are shown in Fig. 1(b) for these three textures. The deviation of uniaxial directions from the film normal increases from textures I to III. As shown in Fig. 1(b), the grains are highly aligned for texture I, i.e., the deviation of the angles between the uniaxial directions of

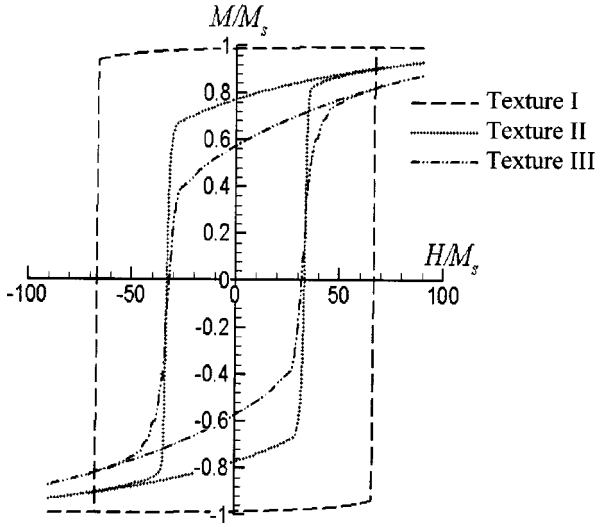

FIG. 2. Hysteresis loops obtained for polycrystalline film with different grain textures.

grains and the film normal is very small. The deviation of these angles for texture II is much larger. Texture III has a random distribution of grain orientations. The corresponding stereographic projections of the grain uniaxial directions are shown in Figs. 1(c)–1(e).

The hysteresis loops of these different textures are shown in Fig. 2. For texture I (very small deviation angle), the hysteresis loop has a nearly square shape with the remanence almost equal to the saturation value, $M_r/M_s=0.98$, and coercivity $h_c=66$. The ratio of the coercivity to the ideal nucleation field is $H_c/H_N^0=0.54$. For texture II with larger deviation angles, the remanence and coercivity are drastically reduced: $M_r/M_s=0.77$ and $h_c=33(H_c/H_N^0=0.27)$. For texture III (almost random orientation distribution), the remanence is further reduced whereas the coercivity remains almost the same as that in texture II: $M_r/M_s=0.57$ and $h_c=32(H_c/H_N^0=0.26)$.

IV. DISCUSSION

Since the only difference between the simulated systems is in misalignment of grains, it is the grain texture that is responsible for the difference in hysteresis loops calculated, in particular, the differences in coercivity and remanence. According to Fig. 2, the remanence decreases monotonically with an increase of the average deviation angle from textures I to III—the greater the misalignment of grains, the less the remanence of the corresponding polycrystalline film. This dependence of the remanence on the grain texture can be explained by the following. The remanence is the average projection of magnetization on the film normal under zero external magnetic field. Because the magnetization in a grain with a greater deviation angle from the film normal has a smaller projection, the texture with greater deviation angle has a smaller value of the total magnetization projection on the normal to the film and, thus, has the smaller remanence.

It is interesting, as follows from Fig. 2, that the coercivity exhibits a different dependence on the grain texture. The coercivity of texture II is less than that of texture I. However,

surprisingly, textures II and III have almost the same coercivity although texture III has a greater deviation angle than texture II. As revealed by our simulations, this different behavior is associated with two competing mechanisms that control the magnetic reversal process, namely, the nucleation of reverse domains and domain wall movement.

The effect of grain texture on the coercivity is associated with the following factors. In our simulations, we neglected the effects of thermal fluctuation and lattice defects in the bulk of the grains on nucleation of reverse domains during switching. We also neglected partial magnetic decoupling of neighboring grains due to the frustration of the exchange energy as well as a change in the magnetic anisotropy within intergranular layers. Under these conditions, the heterogeneous nucleation of reverse domains is mainly associated with the long-range spatially inhomogeneous demagnetization field that is generated by ''magnetic charges'' on the grain boundaries and film external surfaces.

As shown in Figs. 3(a) and 3(c) and Fig. 4(a), the nucleation of reverse domains occurs mostly inside the preferentially oriented grains. The location of the simulated nucleation sites is probably associated with some spatial heterogeneity of the demagnetization field, which is sufficiently long ranged so as to reduce nucleation barriers far from the magnetic charges at the grain boundaries that generate this field.

The nucleation of reverse magnetic domains drastically reduces the nucleation field with respect to the ideal nucleation field, H_N^0, required for homogeneous rotation of the magnetization. It should be noted that, although texture I has a very small average deviation angle, it is still sufficient to provide heterogeneous nucleation; there are always a few grains whose misalignment is sufficient to produce an inhomogeneous demagnetization field that promotes nucleation of reverse domains. The difference between the coercivity H_c of texture I and the ideal nucleation field H_N^0 is caused by reduction of the nucleation barrier for reverse domains caused by this demagnetization field.

The second factor that affects magnetization reversal is domain wall pinning that hinders domain wall movement. Pinning is a local effect associated with frustration of the magnetic anisotropy and exchange interaction by lattice defects. In the case of our model, the only source of such frustration is the grain boundaries where transitions between directions of easy magnetization occur. Since the frustrations depend on grain misalignment, the greater the misalignment between neighboring grains, the more difficult it is for the domain wall to cross the grain boundary, and, thus, the greater the external magnetic field required to push the domain wall through the grain boundary into the neighboring grain. The grain boundary pinning mechanism that controls magnetization reversal and gives rise to an interaction domain structure in nanostructured ferromagnets has been studied experimentally in Ref. 13.

If misalignment between neighboring grains is small, as in texture I, the pinning effect on domain wall movement is also small. On the other hand, the difficulty in nucleation requires the application of a large magnetic field to provide magnetization reversal. In such a situation, a domain wall is not sensitive to the existence of the grain boundaries and moves freely across grain boundaries in a manner similar to movement in a single crystal. This insensitivity to grain

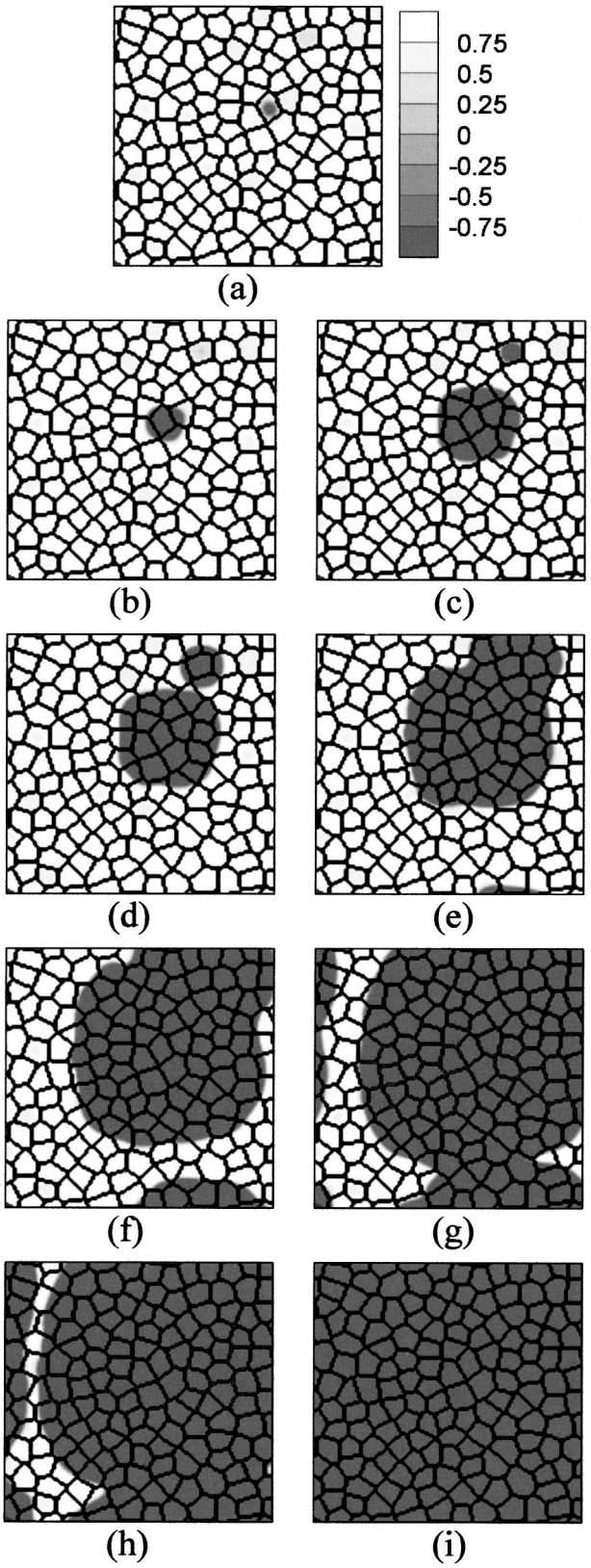

FIG. 3. Evolution of the magnetic domain of the magnetization reversal process for texture I. The gray scale illustrates the Z component of magnetization.

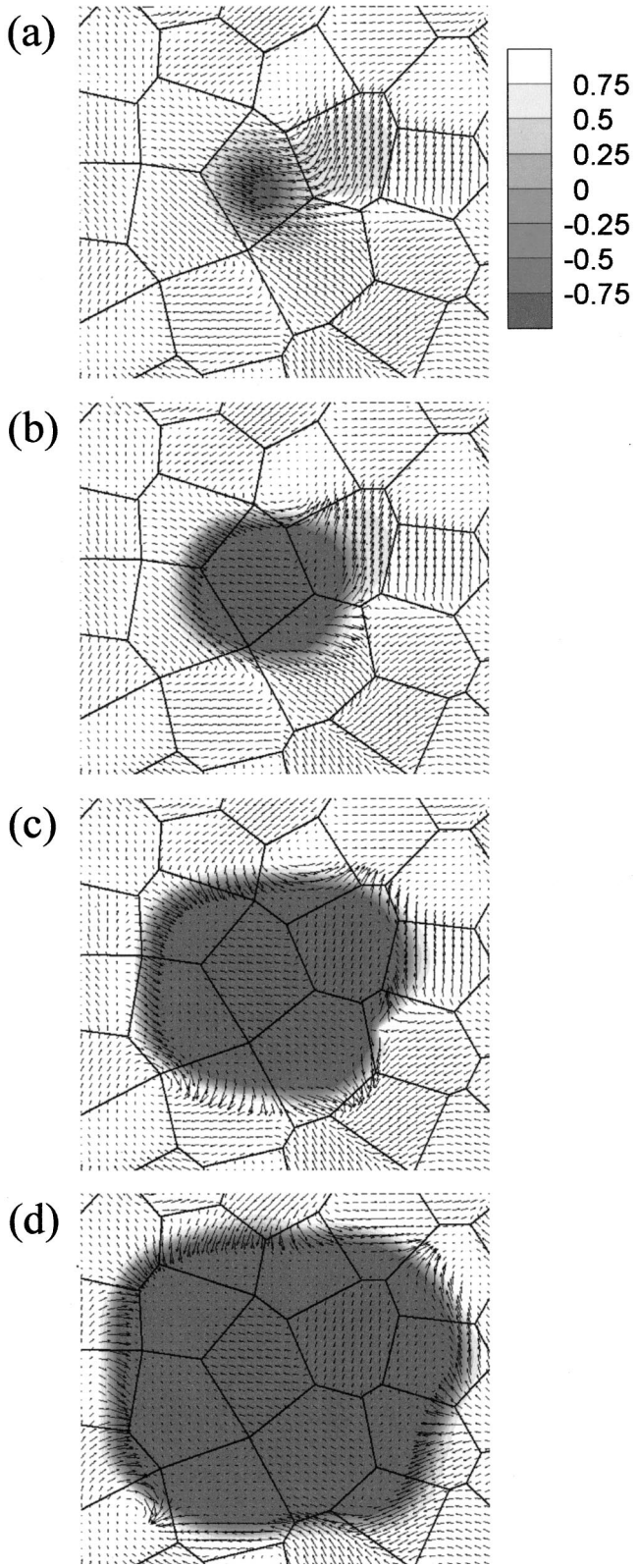

FIG. 4. Close-up view of the vector field of the evolution of magnetization shown in Fig. 3. The *Z* component of the magnetization vector is shown in gray scale and the components in the film plane are shown by a vector.

boundaries is confirmed by our simulation for texture I. The evolution of magnetization during switching in texture I is shown in Fig. 3. Once a domain of a reversed direction nucleates, the domain wall sweeps the entire film, producing complete reversal.

Since the domain wall moves almost without hindrance from the grain boundaries, domain growth occurs nearly isotropically, resulting in a rounded shape of the multigrain area covered by the reverse domains. The coercivity field H_c, in this case, is high, which results in a very steep (nearly square) shape of the hysteresis loop. However, due to heterogeneous nucleation of reverse domains, it is reduced below the ideal value, H_N^0, corresponding to homogeneous rotation of the magnetization.

It is obvious that, as long as grain misalignment exists, frustrations for the magnetization near grain boundaries will also exist. Figure 4 shows a close-up view of the evolution of the domain wall structure as the vector fields of the magnetization evolution corresponding to the process shown in Fig. 3. The perpendicular component of the magnetization vector is shown in gray scale while the in-plane components are shown as vectors. The domain wall is neither pure Bloch nor pure Néel, changes character as it moves across the grains. Figure 4 confirms that the small grain misalignment is not sufficient to pin the domain walls at the grain boundaries at the high external field required for nucleation. This is manifested clearly by the locations of domain walls inside the grains as well as by the isotropic growth of reverse domains over the polycrystalline film that results in a round domain shape.

As discussed above, the greater the deviation angle in the polycrystalline film, the easier the nucleation of reverse domains. This explains the reduction in the coercivity of textures II and III by a factor of 2 compared to that of texture I. On the other hand, the larger the misalignment between neighboring grains, the greater the potency of the grain boundaries to pin the domain walls, and the stronger the barrier is to growth of reverse domains. Nucleation and pinning are separate processes that have opposite effects on the dynamics of magnetization reversal with an increase in grain orientation misalignment. In particular, texture III has a lower nucleation field than texture II, but has higher barriers for domain growth. It is the competition between the pinning of domain wall movement and the easing of nucleation of reverse domains by lowering the nucleation barriers that results in nearly the same coercivity for textures II and III with different grain misalignment.

A prominent feature in the domain evolution of textures II and III is their anisotropic growth compared to the isotropic growth of texture I. For textures II and III, the greater deviation angle eases the nucleation of reverse domains, as shown in Figs. 5 and 6, compared to the case of texture I. Under this condition, magnetization reversal is controlled by domain wall pinning. The domain walls have an energetically more favorable configuration and stay pinned at the grain boundaries. They move across a grain boundary wherever it is able to overcome the local barrier caused by this boundary. The evolution path in this case strongly depends on the local grain orientations. As a result, the domain growth is no longer isotropic: the domains form stripes that percolate the polycrystalline film. The latter is illustrated in Fig. 5 for texture II. Anisotropic growth is even more prominent for texture III because of its greater misalignment angles (Fig. 6).

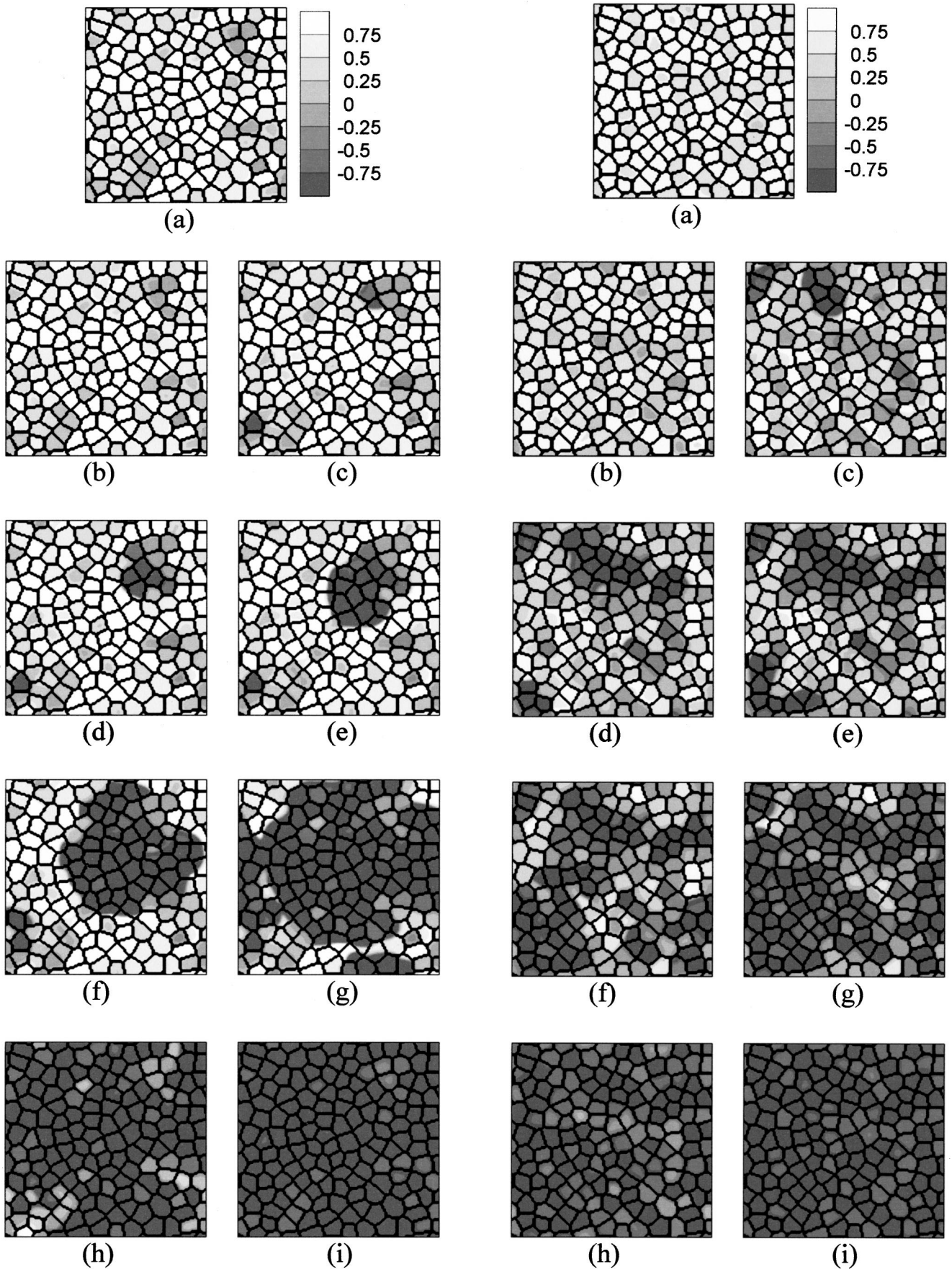

FIG. 5. Evolution of the magnetic domain of the magnetization reversal process for texture II. The gray scale illustrates the *Z* component of magnetization.

FIG. 6. Evolution of the magnetic domain of the magnetization reversal process for texture III. The gray scale illustrates the *Z* component of magnetization.

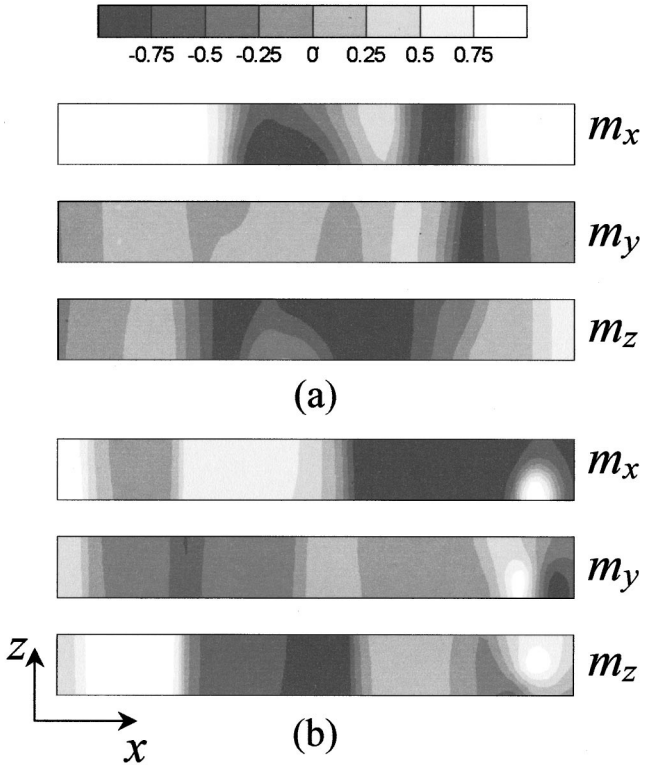

FIG. 7. Portions ($x^*=60-120$) of $X-Z$ cross sections of the magnetization components for the state in Fig. 5(g) at $y^*=$(a) 15 and (b) 22, respectively, where x^* and y^* are the spatial coordinates in units of the computational grid.

The distributions of the three components of the magnetization vector over two typical cross sections of the films are shown in Figs. 7(a) and 7(b). The distribution corresponds to the state illustrated in Fig. 5(g). To visualize the 3D magnetization vector field, we use a gray scale to show the magnitude of the three components in Fig. 7. Figure 7 illustrates the variation of magnetization along the film thickness. It demonstrates that the variation of magnetization along the film thickness cannot be ignored in the computation even for the grain structure that is uniform along the film thickness when the length parameter (δ_W or L_{ex}) is comparable to the film thickness. This is the case for a hard ferromagnetic nanocrystalline FePt film when its thickness is of the order of several nanometers.

The remanence and coercivity are the characteristic features of the hysteresis loop. By controlling these two parameters, different shape hysteresis loops can be obtained, i.e., different magnetic properties can be designed according to the requirement for its application. It should be mentioned that we only considered perfect grain boundaries in this article. In practice, the grain boundaries may be far from perfect. The effect of grain imperfection has been investigated in a study of composite permanent magnets.[14] Films with grains embedded in an amorphous matrix, where the grains are decoupled from each other, are also of interest.[15] As a matter of fact, the model employed in this article requires only minor modification to study systems with imperfect grain boundaries where the magnetization is partially decoupled and magnetic anisotropy is frustrated within intergranular layers. The domain wall pinning effect by lattice defects in the bulk of grains can also be easily taken into consideration. Furthermore, the effect of magnetostriction can also be incorporated into this model by using the PFM approach[7] to characterize the contribution of elastic strain associated with domain structure rearrangement. A more realistic 3D model in which imperfections of grain boundaries, lattice defects, and magnetostriction are taken into consideration would allow one to study a whole spectrum of problems of ferromagnetic media.

V. CONCLUSIONS

Our micromagnetic simulation shows that the magnetic coupling between grains of polycrystalline film significantly affects the morphology of magnetic domains and its response to an external field. The magnetization reversal dynamics strongly depend on the film's texture through the dependence of nucleation and growth of the reverse domains on the grain misalignment. In general, the greater the deviation of the easy axes from the film normal, the smaller the coercivity and remanence of the film. The simulation shows that the remanence and coercivity are affected differently by the grain orientation distribution. The shape of the hysteresis loop may be significantly changed by different grain textures. The remanence exhibits a monotonic dependence on the average deviation angle of the grain texture, whereas the coercivity depends on the deviation angle in a more complicated manner—an increase in grain orientation scattering has opposite effects on nucleation of the reverse domain and on domain wall movement.

Finally, it was shown that magnetic reversal is a collective process that involves the interaction of magnetization in different grains. Texture may significantly affect the morphology and dynamics of expanding reverse domains from one grain to another: the expanding areas of the reverse domains have a round shape for highly textured films whereas they form percolating stripes for films with less texture.

ACKNOWLEDGMENTS

The authors gratefully acknowledge the financial support of NSF under Grant No. DMR-9905725. Computer simulations were performed on NPACI supercomputers.

[1] R. Hertel and H. Krönmuller, IEEE Trans. Magn. **34**, 3922 (1998).
[2] T. Schrefl, J. Magn. Magn. Mater. **207**, 45 (1999); **207**, 66 (1999).
[3] H. N. Bertram and J. G. Zhu, Solid State Phys. **46**, 271 (1992).
[4] J. G. Zhu, in *Magnetic Recording Technology*, edited by C. D. Mee and E. D. Daniel (McGraw–Hill, New York, 1996), Chap. 5.
[5] J. G. Zhu, in *Experimental Methods in the Physical Sciences*, edited by M. D. Graef and Y. Zhu (Academic, New York, 2001), Vol. 36, p. 1.
[6] A. G. Khachaturyan, Fiz. Tverd. Tela (S.-Peterburg) **8**, 2710 (1966); Sov. Phys. Solid State **8**, 2163 (1967); A. G. Khachaturyan and G. A. Shatalov, Sov. Phys. JETP **29**, 557 (1969); A. G. Khachaturyan, *Theory of Structural Transformations in Solids* (Wiley, New York, 1983).
[7] Y. Le Bouar, A. Loiseau, and A. G. Khachaturyan, Acta Mater. **46**, 2777 (1998); Y. Wang and A. G. Khachaturyan, *ibid.* **45**, 759 (1997); Y. U. Wang, Y. M. Jin, A. M. Cuitiño, and A. G. Khachaturyan, *ibid.* **49**, 1847 (2001); Y. M. Jin, Y. U. Wang, and A. G. Khachaturyan, Appl. Phys. Lett. **79**, 3071 (2001).
[8] S. Iwasaki, IEEE Trans. Magn. **20**, 657 (1984).

[9] S. Yamamoto, Y. Nakamura, and S. Iwasaki, IEEE Trans. Magn. **23**, 2070 (1987).
[10] M. E. McHenry and D. E. Laughlin, Acta Mater. **48**, 223 (2000).
[11] T. H. O'Dell, *Ferromagnetodynamics* (Wiley, New York, 1981).
[12] G. Voronoi, J. Reine Angew. Math. **134**, 198 (1908).
[13] H. Okumura, W. A. Soffa, T. J. Klemer, and J. A. Barnard, IEEE Trans. Magn. **34**, 1015 (1998).
[14] R. Fischer and H. Krönmuller, J. Appl. Phys. **83**, 3271 (1998).
[15] S. X. Wang and A. M. Taratorin, *Magnetic Information Storage Technology* (Academic, San Diego, 1998).